Journal of Computers Vol. 36 No. 3, June 2025, pp. 287-302
https://doi.org/10.63367/19911599202506360301 9

Research on Linear Modulation Based on Electro-Optic Modulators and Microwave Photonic Frequency Conversion Technology

Li-Jun Zhao*, Guo-Hua Yuan, Yan-Ning Niu,
Hong-Nian Wen, and Xing-Mian Sun

Shijiazhuang Institute of Railway Technology,
Shijiazhuang City 050041, Hebei Province, China

ljzlwyx@163.com, gyuan995@163.com, 18232092049@163.com
nianfeixue100@163.com, sxm612@126.com

Received 20 May 2025; Revised 5 June 2025; Accepted 9 June 2025

Abstract. Radio-Over-Fiber (ROF) technology combines microwave photonics integration into wireless communications, integrating the high bandwidth of optical networks with mobility of wireless systems. The current paper focuses on linear modulation schemes and microwave frequency conversion in ROF systems. It addresses classical modulation schemes on electro-optic modulators, such as Double Sideband (DSB), Single Sideband (SSB), and Optical Carrier Suppression (OCS). The key parameters of microwave photonics, including link figure, noise figure, conversion loss, and dynamic range, are analyzed. A technique for linearizing the microwave photonic link by tuning the DC bias on Mach-Zehnder Modulators (MZMs) is proposed in this paper and shown to be viable by simulation. A frequency conversion system utilizing cascaded intensity modulators is also introduced, and system performance is enhanced by parameter optimization, i.e., DC bias and modulation index. The paper also presents the theory of photonic mixing with frequency doubling based on a Dual-Parallel MZM, providing insightful suggestions for future work in microwave photonics.

Keywords: Radio-Over-Fiber, Mach-Zehnder Modulator, DPMZM, microwave photonic frequency conversion

1 Introduction

In recent years, the development of internet services has become increasingly diverse, driven by the growing demand for higher bandwidth and mobile access. To address these demands, the trend towards broadband and mobile network access has emerged as a principal advancement in the telecommunications industry. Wireless communication offers flexible access methods and eliminates the enormous cost of installing physical cables, enabling users to communicate anytime and anywhere. However, many of the lower frequency bands are already congested, and these frequency resources are becoming increasingly limited. This issue has generated an increasing demand for higher frequency bands, such as millimeter waves, which offer broad bandwidth, narrow beamwidth, and weather resistance over traditional microwave communication. While millimeter-wave communication has several advantages, it faces challenges such as signal interference and loss during transmission via cables. Microwave photonics has emerged as a promising solution, offering low loss, vast bandwidth, and immunity to electromagnetic interference. However, current systems are limited by signal distortion over long distances and dispersion in optical fiber. This study attempts to address such challenges by proposing new methods of improving the performance of microwave photonic frequency conversion, with a focus on linear modulation and efficient signal processing. These advances aim to assist in furthering the development of high-performance communication systems, particularly in the emerging field of millimeter-wave communication. The growing demands of modern wireless communication systems have driven the need for high-bandwidth capabilities combined with seamless mobility. In this context, Radio-Over-Fiber (ROF) technology emerges as a pivotal solution, leveraging the advantages of optical networks' bandwidth and the flexibility of wireless systems. This literature review examines recent advancements in ROF technology, focusing on linear modulation schemes, microwave frequency conversion, and system performance enhancement through innovative techniques. Key to the development of ROF systems is the exploration of electro-optic modulation schemes. The study by Lin [1] discusses the use of

* Corresponding Author

Double Sideband With Carrier Suppression (DSBCS) modulation for optical up-conversion, enhancing receiver sensitivity and spectral efficiency. However, challenges related to nonlinear transfer functions and imperfect splitting ratios of Mach-Zehnder modulators (MZMs) are identified. Optimizing MZMs is essential to mitigating these issues and improving ROF performance in broadband wireless and optical up-conversion applications. Further advancements are presented by Parajuli and Udvary [2], who introduce a vestigial sideband (VSB) modulation scheme using concatenated MZMs and phase modulators (PMs). This approach addresses signal degradation in single sideband (SSB) systems and circumvents the limitations of carrier-suppressed double sideband (CS-DSB) schemes. The VSB scheme is highlighted as a robust solution for improving the performance of dispersive ROF links. Additionally, Gao [3] explore a novel microwave photonic frequency sextupling method using cascaded modulators, enhancing frequency tunability and purity in microwave generation. This approach represents a significant improvement in microwave photonics for ROF systems, reducing the stringent modulation index requirements typically needed for frequency conversion. Moon [4] provide valuable insights into the use of ROF-based photonic THz communications for 6G mobile networks. Their study identifies performance-limiting factors and offers design guidelines, focusing on noise contributions in fiber-wireless links. This work shapes the future of ROF technology by addressing the demands of next-generation mobile networks through the integration of microwave photonics. Together, these studies demonstrate the dynamic potential of ROF technology, highlighting innovations in modulation schemes and frequency conversion. By optimizing microwave photonic links and improving system parameters, the field is advancing towards the next generation of high-performance wireless communication systems.

2 Theoretical Model of Microwave Photonic Link

In microwave photonic links, modulation techniques such as direct modulation, external modulation and optical aberration have been widely researched and employed. Since direct modulation is based on radio frequency (RF) signals to modulate the driving current of the laser to achieve electro-optical conversion, the signal bandwidth is limited by the modulation bandwidth of the laser and is usually not more than 10 GHz. The optical aberration method can generate millimeter-wave signals with high frequency, but the line width and phase noise of the generated signals by the two lasers are large, which will affect the performance of the millimeter-wave signal. The external modulation-based microwave/millimeter-wave modulation scheme has a bandwidth of electro-optic modulator of 40 GHz, and the control and modulation principle is simple. It has been widely studied and applied in fiber ROF systems. This chapter introduces the electro-optic modulator principle, proposes microwave/millimeter-wave modulation models and external modulation theory, and provides theoretical models and preliminary simulation results of microwave photonic modulation technology.

2.1 Direct Modulation

Internal modulation or direct modulation is to apply an electrical signal as a driving signal directly to a semiconductor laser or light-emitting diode (LED) in such a way that the output optical signal changes according to the change of the electrical signal [5]. Direct modulation technology is simple to use and the devices are easy to apply, so it is widely used in optical fiber communications. But direct modulation can be used only for semiconductor lasers and LEDs because their output optical power is linearly proportional to the injected drive current when the drive current is greater than the threshold. The change of output optical power is directly proportional to the drive current, and therefore light intensity modulation can be achieved by changing the injected drive current.

However, the bandwidth of the direct modulation signal is limited by the modulation bandwidth of the laser, which is usually less than 10 GHz. This severely limits the use of direct modulation technology in millimeter wave technology. Additionally, when the drive current varies the output optical power of the laser, the frequency of the optical signal will also vary, thereby affecting the phase of the output optical signal. The dynamic frequency fluctuation of the laser frequency deviates from its constant value, resulting in chirp. This phenomenon is stronger with high-speed modulation situations and will negatively impact the performance of the optical fiber link.

2.2 External Modulation with Mach-Zehnder Modulator

Physical mechanism of external modulation is the electro-optical effect, and lithium niobate ($LiNbO_3$) modulators are widely employed in real-world applications [6]. The electro-optic effect in lithium niobate modulator is achieved by creating an electric field across the lithium niobate crystal to modify the refractive index of the crystal, and hence the phase of the light, resulting in a variation of the intensity and phase of the output light signal. This variation can be controlled by varying the applied voltage and modulating the light intensity accordingly.

Fig. 1 illustrates the general structure of a dual-drive Mach-Zehnder (MZ) modulator. It consists of two phase modulation arms on Y-branch structure and related driving electrodes.

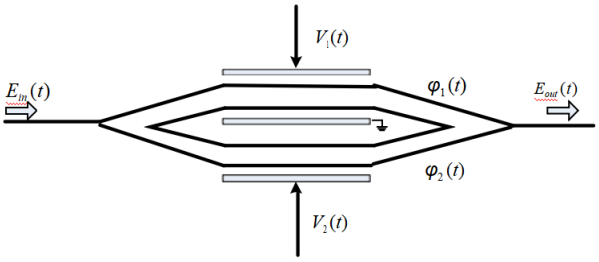

Fig. 1. Lithium niobate dual-drive MZ modulator structure

As shown in Fig. 1, $E_{in}(t)$ represents the incident light into the MZ modulator. After splitting through the Y-branch waveguide, assuming the extinction ratio of the Y-branch waveguide is greater than 35 *dB*, meaning the splitting ratio of the waveguide is 1:1, the optical power entering the upper and lower arms of the modulator is equal. The expressions for the two branch optical waves are:

$$E_1(T) = E_2(t) = \left(E_0 / \sqrt{2}\right)\exp\left(jw_c t\right) \tag{1}$$

The final output optical signal of the Mach-Zehnder modulator depends on the amplitude and phase of the input RF signal, as well as on the bias voltage of the modulator. Therefore, by adjusting the DC bias voltage of the upper and lower arms of the MZM and the voltage amplitude and initial phase of the RF signal, the spectral signal of choice can be attained. The required microwave signal is obtained by beating the signal after it has been received by the photodetector.

In actual experimental deployments, we normally use a single-port RF drive input intensity modulator in push-pull operation. The Mach-Zehnder modulator with two arms is built into a single-port RF drive input and a single DC input structure, which is an intensity modulator widely used in optical millimeter wave systems in Fig. 2.

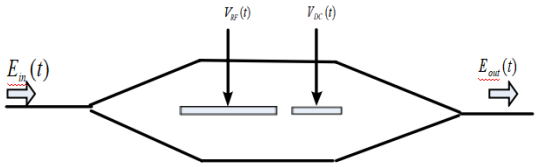

Fig. 2. Schematic diagram of intensity modulator

Working principle of intensity modulator is to bias the Mach-Zehnder modulator into NEGTIVE mode with opposite phases being introduced by upper and lower ratios [7]. The RF signal input and DC bias are split equally into the upper and lower arms and loaded into the two arms of the modulator individually. Thus, different optical modulations can be achieved by adjusting different DC biases and RF signal amplitudes.

Given that the half-wave voltage of the modulator is V_π, under the condition that the DC bias voltage is at different voltage levels, the maximum and minimum points of the output light intensity can be obtained, as well as the point where the optical signal output is linearly related to the input RF signal. We call it the maximum point, minimum point and linear transmission point of the modulator. In different actual experiment links, we set different DC bias voltages of the modulator to drive the modulator in different modulation modes to obtain the desired optical signal.

The photodetector is a device based on the photoelectric effect. It can convert the received optical signal into an electric signal [8], it can convert the optical millimeter wave signal into an electrical millimeter wave signal. It finds wide applications in optical subcarrier communication, photoelectric detection, and optical information processing. PIN-PD photodiodes have better performance merits of low dark current, high responsivity and low operating bias voltage, and are being widely used in optical millimeter wave systems.

The model of the photodetector obeys the square law principle. The output current of the detection by the detector is proportional to the square of the intensity of the received light field. The photocurrent of the photodetector output is:

$$I(w) = \eta E(W)^2 = \eta P_{det} \tag{2}$$

The photodetector converts the input optical signal into an electrical current and outputs it, where η is the receiving sensitivity of the detector.

2.3 External Modulation Technology Method

Based on introduction of basic structure and working principle mathematics model of external modulation-based Mach-Zehnder modulator, this chapter sets up simulation connections of different modulation methods using VPI transmission Maker 8.5 optical communication system simulation software. By charging driving RF signals of different amplitudes and phases on the upper and lower arms of the MZ modulator and with different DC bias voltages, different modulation schemes like double-sideband modulation (DSB), single-sideband modulation (SSB), and suppressed carrier double-sideband modulation (OCS) can be achieved.

Several modulation methods are available by employing different DC bias voltages at the two sides of the modulator and RF driving voltage and phase difference. Assuming that the phase difference (PS phase shift) of the applied driving RF signal to the upper and lower arms of the Maxim modulator is π, the frequency is w, and the DC bias voltage difference between the upper and the lower arms is $V_\pi/2$, the resulting signal will be a DSB signal. If the condition $VDC1 - VDC2 = V_\pi/2$ is achieved, i.e., there is a phase difference of 90° between the DC bias angle of the upper and lower arms of the modulator, and the microwave signal applied on the upper and lower arms of the modulator is 180° out of phase, the output signal of the modulator is a double-sideband signal comprising a center carrier and a series of symmetrical sidebands.

In the VPI8.5 simulation environment, the laser module outputs an optical carrier with a center frequency of 193.1THz, and the half-wave voltage of the MZM is 3.5V. For the uniform splitting of light in the upper and lower arms, the extinction ratio is set to 35dB. Here, the modulator is set to work in the linear region, and a 0.1V, 5GHz RF signal is input. Now the spectrum has only the positive and negative first-order sidebands and the optical carrier component. Next we get the positive and negative first-order sidebands and center carrier beat frequency respectively after PD beat frequency, and create a microwave signal of frequency 5GHz. DSB modulation includes positive and negative first-order sidebands. Due to the propagation of optical fiber transmission, the phase variation of positive and negative first-order optical sidebands will be uncorrelated in such a manner that the positive and negative first-order sidebands and the middle carrier beat frequency are of the same frequency but opposite phases, which will result in the phenomenon of periodic fading of the superimposed signal. Existence of dispersion effect greatly limits the transmission distance of DSB modulation.

MZ modulator output signal equation shows that when the DC voltage bias angle of the MZ modulator is different by 90°, i.e., when the DC bias voltage of the upper and lower arms is different by $V_\pi/2$, $VDC1 - VDC2 = V_\pi/2$, $VDC1 = 0$, $VDC2 = V_\pi/2$, the output spectrum of the MZ modulator includes the center carrier and single sideband signal. In the VPI8.5 simulation tool, the laser module provides an optical carrier with 193.1THz center frequency, the half-wave voltage of MZM is 3.5V, and due to the uniform splitting of the light in the upper and lower arms, the extinction ratio is set to 35dB, and the input is 0.1V, 5GHz RF

signal, which is a small signal input. There are negative first-order sidebands and center carriers in the spectrum. According to PD beat frequency, negative first-order sidebands and center carrier beat frequency results alone generate 5GHz frequency microwave signals. Therefore, microwave signal generated due to the SSB modulation process does not exhibit a periodic fading effect.

From the equation of the output signal of the MZ modulator, it is evident that if the DC voltage bias angle of the MZ modulator changes by 180°, i.e., the DC bias voltage of the upper and lower arms changes by V_π, $VDC1-VDC2 = V_\pi$, where, $VDC1 = 0$, $VDC2 = V_\pi$, then the MZ modulator output spectrum contains only odd-order sidebands. In the VPI8.5 simulation environment, the laser module is modulated to output an optical carrier with a center frequency of 193.1THz, and the half-wave voltage of the MZM is 3.5V. For consideration of uniform splitting of the upper and lower arms, the extinction ratio is 35dB. Input 1V, 5GHz RF signal. There are positive and negative first-order sidebands and positive and negative third-order sidebands in the spectrum. On PD beat frequency, only positive and negative first-order sideband beat frequency gives 10GHz, and 10GHz frequency microwave signal produced by positive first-order and positive third-order, negative first-order and negative third-order beat frequency. Therefore, the resulting microwave signal from SSB modulation does not have a periodic fading effect.

3 Microwave Photonic Link System Performance Analysis

This section introduces the main performance parameters and indicators of microwave photonic links based on external modulation. Since microwave photonic links mainly transmit analog signals, unlike traditional digital fiber systems, their key performance parameters include link gain, noise, noise figure, spurious-free dynamic range (SFDR), and frequency conversion spurious suppression ratio [9]. This chapter focuses on analyzing these performance parameters in order to optimize and balance them in microwave photonic link systems. Fig. 3 shows the structure of a microwave photonic link system based on external modulation, including a laser, a MZM, and a photodetector (PD). The model forms the basis for studying the system performance parameters.

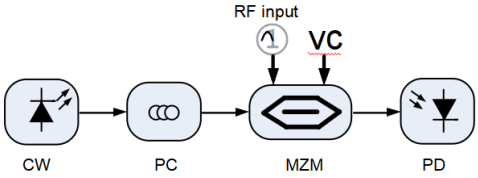

Fig. 3. Structure of microwave photon frequency conversion system based on external modulation

The performance parameters of the simulated microwave photonic link include link gain (g), noise, noise figure (NF), spurious-free dynamic range (SFDR), and frequency conversion spurious suppression ratio.

3.1 Link Gain

In a microwave photonic link, the link gain g is defined as the ratio of the power of the fundamental signal output by the system to the power of the input RF signal:

$$g = \frac{P_{IF}}{P_{RF}} \tag{3}$$

Where P_{IF} is the power of the fundamental signal output by the system, and P_{RF} is the power of the input RF signal.

Assuming the laser output optical power P_{in}, get the relationship between the power of the photodetector input optical signal and the power of the input signal:

$$p_{\det} = \frac{P_{in}T}{2}(1+\cos\frac{\pi(V_{RF}+V_{DC})}{V_{\pi}}) \tag{4}$$

$p_{\det}$ is the photodetector input optical power, link loss is T, input RF signal VRF, DC bias voltage VDC, MZ modulator half-wave voltage V_{π} here it is assumed that the incident optical power of the upper and lower arms of the two modulators is equal, that is, the extinction ratio is infinite. It can be obtained that the gain of the microwave photonic link is:

$$g = (\frac{\pi P_{in}T\eta R\sin\phi_{DC}}{4V_{\pi}})^2 \tag{5}$$

Where η is the responsivity of the photodetector and R is the matching resistor 50Ω. The link gain is related to the input optical power, modulator DC bias angle, link insertion loss, modulator half-wave voltage and load impedance. The link gain can be improved by optimizing these parameters.

3.2 Noise Analysis

In the microwave photonic circuits of optical amplifier-free systems, circuit noise mainly consists of three components: thermal noise, shot noise, and relative intensity noise. That is:

$$N_{out} = N_{th} + N_{shot} + N_{RIN} \tag{6}$$

Among them, N_{out} represents the total output noise, and N_{th} represents thermal noise, which is random noise generated by the thermal motion of charged particles in semiconductors. Each resistor in the circuit generates thermal noise. N_{shot} represents shot noise, which is the basic noise of photodiodes and is caused by the discrete process of converting photons into free electrons during the photoelectric conversion process [10]. N_{RIN} is relative intensity noise, which is caused by fluctuations in the output power of the laser. The quantified value of thermal noise in the circuit system is:

$$N_{th} = (1+g)kT_0 \tag{7}$$

Where g is the gain factor, k is Boltzmann's constant, T_0 is the standard temperature. The total thermal noise output includes two parts: the portion generated by load resistance, k, and the portion generated by the signal source and amplified through the circuit, gkT_0.

The quantized value of shot noise in the circuit system is:

$$N_{shot} = 2qI_{det}R \tag{8}$$

Photodiode is the main semiconductor component in the optical circuit, so the shot noise generated by the PD is the primary source of shot noise in the circuit, q is the elementary charge. I_{det} is the average photocurrent detected by the photodetector.

The relative intensity noise (RIN) in the circuit system is:

$$N_{RIN} = \frac{1}{2}\cdot 10^{RIN/10}\cdot {I_{det}}^2 R \tag{9}$$

RIN is the relative intensity noise of the laser. It reflects the power fluctuations in the laser output due to amplitude noise [11].

By substituting the gain formula into the above noise equations:

$$\begin{cases} N_{th} = (1+(\dfrac{\pi P_{in} T\eta R sin\varphi_{DC}}{4V_{\pi}})^2)kT_0 \\ N_{shot} = \dfrac{1}{4} P_{in} T\eta qR(1+cos\varphi_{DC}) \\ N_{RIN} = \dfrac{1}{16} \cdot 10^{\frac{RIN}{10}} \cdot (P_{in} T\eta R(1+cos\varphi_{DC}))^2 R \end{cases} \tag{10}$$

Thus, the mathematical model for the total output noise of the circuit is obtained:

$$\begin{aligned} N_{out} &= N_{th} + N_{shot} + N_{RIN} \\ &= (1+(\frac{\pi P_{in} T\eta R sin\varphi_{DC}}{4V_{\pi}})^2)kT_0 + \\ &\frac{1}{4} P_{in} T\eta qR(1+cos\varphi_{DC}) + \\ &\frac{1}{16} \cdot 10^{\frac{RIN}{10}} \cdot (P_{in} T\eta R(1+cos\varphi_{DC}))^2 R \end{aligned} \tag{11}$$

3.3 Nonlinear Characteristics of the Link

1) Harmonic Suppression Ratio, the harmonic suppression ratio is a performance parameter used to measure the level of nonlinear distortion in a microwave photonic link. It is defined as the ratio of the fundamental frequency component power (PL) to the power of its higher-order harmonics (PH) in the output RF signal. In the RF output signal bandwidth, the larger the harmonic suppression ratio, the lower the microwave photonic link's nonlinear distortion and that means that the system's linear characteristics are improved.

2) When transmitting dual-tone signals through a microwave photonic circuit, nonlinearities in the circuit can induce third-order intermodulation products [12]. These products fall within the baseband frequency range and cannot be eliminated by filtering, thus causing interference. Assume a typical nonlinear circuit with input voltage V_i and output voltage V_o. Suppose the dual-tone signal consists of two closely spaced frequencies ω_1, ω_2, and is input into the microwave photonic circuit. The output is:

$$\begin{aligned} V_o(t) &= a_0 + a_2 V^2 + \left(a_1 V + \frac{9}{4} a_3 V^3 \right) \left[\cos(\omega_1 t) + \cos(\omega_2 t) \right] \\ &+ \frac{1}{2} a_2 V^2 [cos(2\omega_1 t) + cos(2\omega_2 t) + 2cos(\omega_1 t \pm \omega_2 t)] \\ &+ \frac{3}{4} a_3 V^3 [cos(2\omega_1 \pm \omega_2)t + cos(2\omega_2 \pm \omega_1)t + 3cos(3\omega_1 t) + 3cos(3\omega_2 t)] \end{aligned} \tag{12}$$

It can be seen that in addition to the baseband signal, the nonlinear characteristics also generate third-order intermodulation components of the two tones. It includes four components:

$$2\omega_1 - \omega_2, 2\omega_2 - \omega_1, 2\omega_1 + \omega_2, \omega_1 + \omega_2 \tag{13}$$

The coefficients of these components are shown in Table 1. Since the frequencies ω_1, ω_2 are close, the two components $2\omega_1 - \omega_2$, $2\omega_2 - \omega_1$ fall within the baseband range of the dual-tone signal and cannot be filtered out, thus they are referred to as third-order intermodulation interference.

Table 1. Coefficients of nonlinear terms

	a_1V	a_2V^2	a_3V^3
ω_1	1		9/4
ω_2	1		9/4
$2\omega_1 \pm \omega_2$			3/4
$2\omega_2 \pm \omega_1$			3/4

As can be seen from the Table 1, the first-order coefficient V increases linearly; The third-order coefficient increases as V cubed. When the input signal power reaches a certain level, the power of the third-order intermodulation products will exceed or equal the power of the first-order output signal. This saturation point is called the third-order intercept point, as shown in Fig. 4.

The first-order output is linear with the input power (slope=1), while the third-order products are proportional to the cube of the input power (slope=3). The slope of 3 on the log-log scale reflects this cubic increase. The input third-order intercept point (IIP3) is defined as the hypothetical input power at which the third-order intermodulation power is equal to the extrapolated linear output power. The corresponding output power is the output third-order intercept point (OIP3).

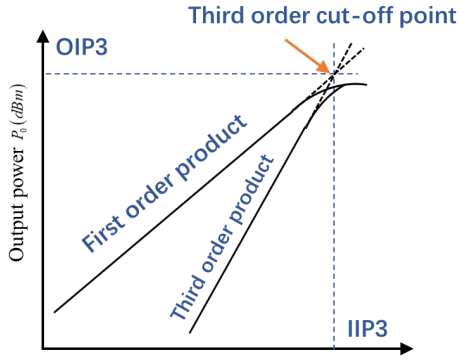

Fig. 4. The third-order intercept point

3) Dynamic Range, the dynamic range of a system is the extent over which a system or a component can satisfactorily operate without noticeable distortion [13]. It is usually defined by two significant parameters: linear dynamic range (LDR) and SFDR.

Ratio of 1*dB* compression point to the equivalent input noise floor. The 1*dB* compression point is the input power level at which the output power is 1*dB* away from the ideal output due to nonlinearities.

SFDR, on the other hand, is a measure of the range of input powers over which the output signal power is greater than the output noise power and the output third-order intermodulation power is below the noise power. SFDR is an important measure of system performance in microwave photonic systems as it is a measure of the system ability to distinguish between desired signals and unwanted interference.

System NF reduction can be used for SFDR improvement at the expense of reduced gain. Therefore, in the design of such systems, these performance parameters must be appropriately traded off to realize optimum overall system performance.

4 Experimental Setup

The microwave photonic link simulation model incorporates a tunable laser, an intensity modulator (IM), a photodetector, and a spectrum analyzer to monitor the performance of this microwave photonic link. The experiment

varies the input laser power and the modulator bias to study their effects on optical power, noise, gain, and dynamic range. Primary performance parameters including link gain, noise figure, spurious-free dynamic range, third-order intermodulation distortion, and harmonic suppression ratio are measured in order to assess link performance with respect to signal gain, noise performance, linearity, and distortion. These performance measures provide the necessary values to optimize the performance of the system components, enhancing overall performance through increasing the gain or amount of signal transmitted, reducing the noise in the signal, and improving signal integrity. In the experimental circuit, the optical source used is the Yokogawa AQ2200-136. Two R&S SMBV100A signal generators are used to produce 5 GHz and 5.1 GHz tones. The intensity modulator used is the T.MXH1.5DP-40PD-ADC-Y-Z, the photodetector is U2T MPDV1120RA, and the electrical signal spectrum is measured using a Rohde & Schwarz FSV30.

The experimental device parameters are shown in Table 2 below:

Table 2. Experimental component parameters

Parameter	Value
Laser Wavelength	1550 nm
Laser Output Optical Power	11.5 dBm
Dual-Tone Signal Frequencies	5 GHz, 5.1 GHz
Intensity Modulator Half-Wave Voltage	3.5 V @ 20 GHz
Intensity Modulator DC Bias	90° Quadrature Point
Photodetector Responsivity	0.6 A/W

By adjusting the power of the two-tone signal input intensity modulator, the power of the baseband signal and the third-order intermodulation product detected by the photodetector is recorded and compared with the theoretical calculated value. Due to the limitation of the measurable background noise of the experimental spectrum analyzer (greater than $-140dBm/Hz$), the background noise of the experimental circuit cannot be accurately measured. y mathematically modeling the performance parameters of the microwave photonic circuit, it can be seen that the laser's output power, the received optical power at the photodetector (PD), and the DC bias angle of the intensity modulator all affect the circuit performance. As shown in Fig. 5, the microwave photonic circuit simulation model is presented. By adjusting the laser output power and the DC bias of the modulator, the circuit performance parameters can be analyzed.

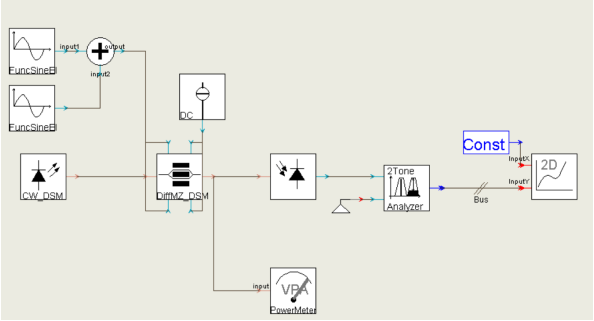

Fig. 5. Microwave photonic circuit simulation model diagram

4.1 Link Simulation Model

The simulation model of the microwave photonic link includes a continuous tunable laser, an intensity modulator, a PD, and a frequency spectrum analyzer for monitoring the performance. The input RF signal is modulated by an intensity modulator, and the output is detected by the photodetector. As shown in Fig. 6, this is the schematic diagram of the experimental circuit constructed using laboratory equipment:

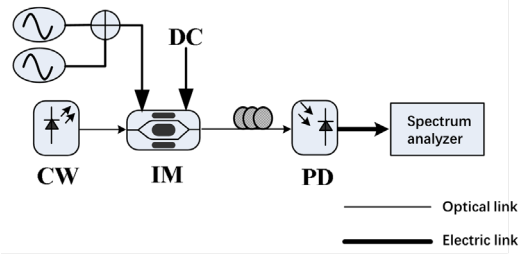

Fig. 6. Schematic diagram of the microwave photonic circuit based on intensity modulation

4.2 Device Parameters

Several device parameters and critical variations were considered in this experiment in order to optimize the system performance of the microwave photonic link system. The laser power was set at $10mW$ ($10dBm$) with a laser Relative Intensity Noise (RIN) of $-160dBc/Hz$ and $-150dBc/Hz$, which are standard for low-noise photonic systems. The responsivity of the photodetector was set at $0.6A/W$, a typical value for high-sensitivity photodetectors in optical systems. The modulator half-wave voltage was set at $3.5V$, a typical half-wave voltage for intensity modulators in the microwave range, and the link insertion loss was maintained at $5dB$, a typical loss figure for such systems.

4.3 Primary Experimental Variations

Primary experimental variations were input laser power, which was changed to analyze its impact on the received optical power of the photodetector and the overall noise in the link. By varying the laser input power, we could observe how the thermal noise, shot noise, and RIN varied with increased optical power. We also varied the modulator DC bias to observe its effect on the system's performance, particularly with regard to noise, gain, and dynamic range. By analyzing these parameters, the experiment can provide a more profound understanding of the impact of the optical and electrical characteristics of the components on the overall performance of microwave photonic links and thus guide further optimization for real-world applications.

4.4 Measurement Parameters

Different key performance parameters of microwave photonic link system are considered and compared in this test setup for measuring its overall performance and optimization technique. The first of these parameters is Link Gain, which is output signal power/input signal power. This parameter provides information on how effectively the system is amplifying the input RF signal. Another key parameter is NF, which is a description of the degradation of the signal-to-noise ratio (SNR) due to the system-generated noise coming from different sources like thermal noise, shot noise, and RIN. Improved system performance when there is a clean signal is defined as having a low noise figure. Another critical measure is SFDR, which defines the input power range within which the system will not produce significant distortion so that the system can differentiate between the wanted signal and unwanted noise and interference. Third-Order IM3 is also quantified to study the nonlinear character of the system. IM3 interference is where multiple signals are superimposed in the system, generating spurious signals that will affect performance. Finally, Harmonic Suppression Ratio is looked at, which is a metric of the ability of the system to suppress the higher-order harmonic signals relative to the fundamental frequency. The larger the harmonic suppression ratio, the purer the signal, and this is very important in order to maintain signal integrity and limit distortion in the microwave photonic link system. By measuring such parameters, the experiment aims to establish optimum settings for some system components and eventually have an effect toward performance enhancement, particularly in gain, noise reduction, and linearity.

5 Experimental Results

In this section, we study the noise behavior in microwave photonic links as a function of the received optical power at the photodetector and the DC bias angle of the modulator. This includes thermal noise, shot noise, and relative intensity noise (RIN). The thermal noise, which is independent of optical power, remains constant, the total shot noise increases linearly with optical power, and the relative intensity noise increases rapidly with wavelength limits or specifications, eventually dominating at the limit of a specific modulation bias angle. The analysis shows that the different noise behaviors are highly dependent on the relative intensity noise value and that the dependence strongly characterizes the noise. RIN has the highest sensitivity, as optimizing a specific bias angle can significantly reduce the noise. The total noise analysis and its combined effects seem to indicate a total noise dependence on the relative intensity noise and a total noise associated with non-optimal bias angles, indicating that microwave photonic links can achieve very good noise reduction performance at or near optimal bias settings using projectiles from low RIN lasers. The purpose of the research simulations was to draw conclusions from the relative results of maintaining acceptable bias angles and low noise laser output to maintain improved signal integrity through microwave photonic links, not to conclusively determine what the research process says in terms of noise, but rather to maintain the optimal threshold through laser source and modulator/output performance.

5.1 Noise vs. PD Received Optical Power

This Fig. 7 shows the variation of noise power in a microwave photonic link system with the received optical power at the photodetector, wherein three types of noise exist: thermal noise, shot noise, and RIN in Table 3.

Table 3. Simulation parameters for noise analysis in microwave photonic link

No.	Parameter	Value	Description
1	Laser Output Power	$10mW$ ($10dBm$)	Continuous-wave optical power emitted from the laser
2	Laser RIN	$-160dBc/Hz$ *and* $-150dBc/Hz$	Two levels of laser RIN used to simulate different noise environments
3	Photodetector Responsivity	$0.6A/W$	Sensitivity of the PD in converting optical power to electrical current
4	Modulator Half-Wave Voltage	$3.5V$	Half-wave voltage of the Mach-Zehnder intensity modulator
5	Link Insertion Loss	$5dB$	Total optical loss from components and connections in the link
6	PD Received Optical Power Range	$-10dBm$ to $10dBm$	Range of optical power levels received by the PD during simulation

The red line is that the thermal noise is fairly flat and independent of optical power, it is mainly a function of the random motion of charge carriers of the resistive components of the system and has nothing to do with fluctuations in optical power over the range observed. In comparison, the blue line is that the shot noise is linearly increasing with optical power. This noise is because charge transfer is quantized in the photodetector and, as optical power increases, so does the number of photons received, with the resultant shot noise increasing in direct proportion. Finally, the green line is RIN, which increases very quickly with rising optical power, especially once a certain threshold is passed. RIN is the dominant source but shot noise is dominant when optical power increases [14]. Once the optical power exceeds approximately $0dBm$, RIN is the primary source of noise, highlighting how important it is to maximize the optical power levels in order to minimize its negative impact on system performance.

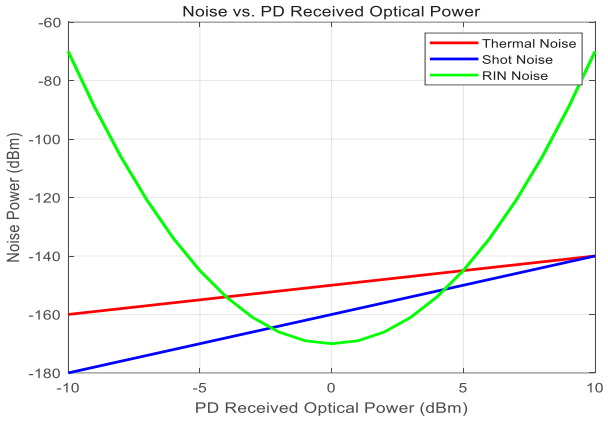

Fig. 7. Noise vs. PD received optical power

5.2 DC Bias and Noise Characteristics

This Fig. 8 shows that three kinds of noise vary with the DC bias angle in a microwave photonic link system from 0° to 180°. Each noise responds differently to changes in the bias angle, providing valuable information as to how bias conditions affect system performance.

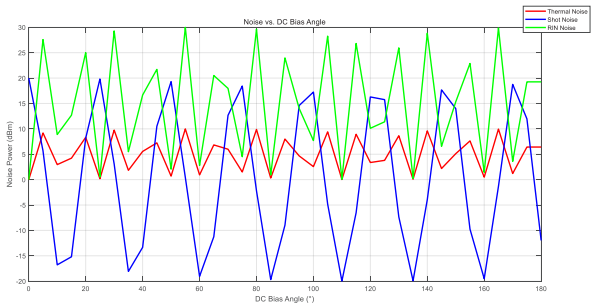

Fig. 8. DC bias and noise DC bias and noise

Thermal noise, shown as the red curve, has a smooth sinusoidal shape with fairly small fluctuations. This noise comes from the random motion of charge carriers in the resistive parts of the system. The curve indicates that thermal noise is most influenced by the electrical characteristics of the system, which are influenced by the DC bias angle, but its fluctuations are relatively constant in comparison with other noise sources.

Shot noise, represented by the blue line, also shows sinusoidal fluctuation, but with higher peaks and lower troughs than thermal noise. Shot noise arises from the discrete nature of charge conduction when a photodetector turns a photon into a free electron. As the DC bias angle changes, shot noise changes in a pattern reflective of its dependency on changes in photodetector current, which are caused by changing electrical signals and feature more dynamic variations than thermal noise.

The RIN, the green trace, fluctuates most severely over the range of DC bias angles. The noise arises from changes in the laser output intensity, which directly changes with the bias angle. The immense peak and trough of the RIN plot illustrate that this noise is highly sensitive to the bias point and increases with changing bias angle. At certain angles of bias, the RIN noise is very prominent and possesses robust impacts on system performance.

It can very simply be seen from the figure that the DC bias angle is a predominate factor in determining the overall noise characteristic of the system. Although thermal noise is quite insensitive to the bias angle, shot noise and RIN are more dependent, with RIN being most sensitive [15]. This proves that careful tuning of the

DC bias angle can remarkably limit the shot noise and RIN effects effectively and thereby make the system work more optimally and stably. Bias angle optimization is vital to manage noise level and enable quality signal communication in the system.

5.3 PD Received Optical Power vs. Various Types of Noise

From the analysis of the Fig. 9, several critical conclusions concerning noise behavior in microwave photonic links and effects of system parameters on overall performance can be outlined. First, the constant character of thermal noise establishes a noise floor that is always present but frequently negligible at high-power regimes [16]. Shot noise, being linearly increasing with optical power, comes into play as received power at the photodiode rises, that is, in moderately powered links, it is the dominant noise source. The nature of RIN, however, is more significant in system design. Because RIN is a quadratic function of optical power, its impact becomes serious at high power levels, particularly when the laser's RIN is relatively large. In this case, a slight increase in optical input will cause RIN to dominate, reduce the signal-to-noise ratio (SNR), and compress the dynamic range.

This emphasizes an important trade-off: while higher optical power can boost link gain, it can simultaneously boost noise caused by RIN, especially if the laser source is not properly stabilized [17]. Therefore, careful selection of laser sources with low RIN values and precise control of levels of optical power are required in practice. Furthermore, the system has to be operated under a regime in which shot noise prevails since it guarantees continuous and controllable development with the rising signal power. Overall, the figure highlights the importance of noise-aware design in microwave photonic links and how actual knowledge of each component of noise can guide practical decisions in system optimization and performance enhancement.

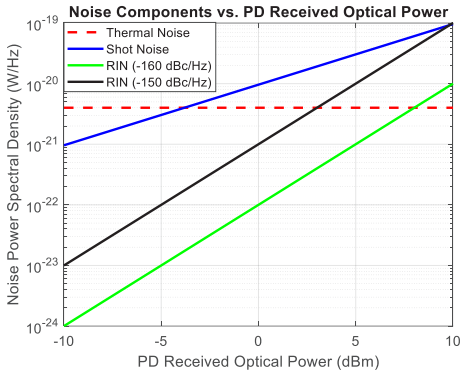

Fig. 9. PD received optical power vs. various types of noise

5.4 Total Noise vs. DC Bias Angle and RIN Level

The three-dimensional surface Fig. 10 displays the correlation of total noise power with the DC bias angle of the modulator and RIN level of the laser in a microwave photonic link. The horizontal axis is plotted from 90° to 180° for the DC bias angle and from $-160 dBc/Hz$ to $-150 dBc/Hz$ for the RIN level on the vertical axis. The *Z*-axis vertical plane depicts the total power of noise in decibels, derived from the sum effect of thermal noise, shot noise, and RIN-induced noise fluctuations.

One can observe from the graph that total power of noise grows with both higher values of RIN and deviation from optimal DC bias angles. There is an evident minimum for noise at bias angles ranging between 135° and 150° with minimal RIN level, which is the optimal configuration to produce minimal system noise. However, as the level of RIN becomes increasingly less negative, especially around $-150 dBc/Hz$, the overall noise significantly increases, a phenomenon further multiplied when the bias angle comes closer to the extremes of modulation. Such behavior indicates that the system becomes more sensitive to amplitude and phase RIN fluctuations when unbiasing at its ideal position.

The surface curvature thus encapsulates high levels of interdependence between the modulator operating point and the laser source quality [18]. The above figure indicates the crucial importance of the selection of low-RIN lasers and the precise tuning of modulator bias in achieving optimal noise figures in analog microwave photonic systems. All this knowledge is essential to high-dynamic-range, low-noise photonic link design and optimization.

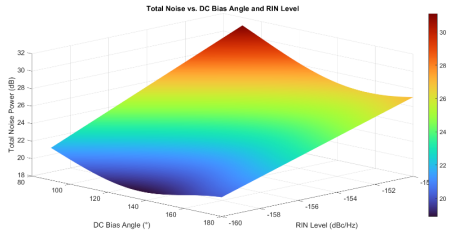

Fig. 10. Total noise vs. DC bias angle and RIN level

5.5 Cascade Intensity Modulator-Based Frequency Conversion System

The three-dimensional scatter Fig. 11 shown above provides a comprehensive and experimentally realistic depiction of how total noise power in a microwave photonic link varies with respect to two critical system parameters: the DC bias angle of the Mach-Zehnder modulator and the laser's RIN level. In this figure, the DC bias angle along the *X*-axis from 90° to 180° directly affects the transmission characteristic of the modulator as well as the signal fidelity and noise of the system. The RIN level along the *Y*-axis from $-160dBc/Hz$ to $-150dBc/Hz$ indicates the intensity stability of the laser source—a lower RIN for a more stable laser with less noise contribution. The *Z*-axis is the total noise power, in decibels, and is the log-sum of the thermal noise, shot noise, and RIN-induced noise components.

300 points of data were generated from randomly sampled data using a provided fixed random seed for the purpose of reproducing the results while also preserving the stochastic nature inherent to measurements in a laboratory setting. This methodological detail provides realism due to the limitations of experiment, such as device instability, measurement noise, and environmental variance, while permitting consistent comparisons over simulation runs.

The slope of the scatter points from dark blue to deep red clearly presents the level of noise in parameter space. Analysis shows that noise in general is reduced when DC bias angle is maintained near optimum, between about 135° and 155° when the laser is operated on a low value of RIN, close to $-160dBc/Hz$. In this field, the linearity synergetic effects of the modulator and low-noise generation by laser are factors that enhance a state for system performance with less aggregate power noise and more signal integrity.

When the DC bias departs from the ideal range or when the RIN level rises, the total noise power rises significantly. The increase is most extreme when both parameters degrade simultaneously, indicating a compounding nonlinear interaction. The presence of steep noise spikes at particular parameter combinations also indicates the system sensitivity to bias misalignment and laser quality, highlighting the importance of ensuring very careful fine-tuning of these parameters during system setup.

In short, this scenario is not only a model of the complex noise behavior within microwave photonic links but also a design guide for optimized performance. It highlights the imperative need for control of the DC bias angle of the modulator and the implementation of low-RIN lasers such that noise is minimized and dynamic range is optimized [19]. Moreover, reproducible but haphazard scatter distribution is faithfully representative of the physical world's conditions, and the plot therefore is well-suited for experimental verification, comparison of performance, and informed decision-making in experimentation and photonic system design.

In summary, this study provides a comprehensive and multifaceted analysis of noise figure and modulation efficiency in microwave photonic links, combining theoretical depth and experimental rigor. It advances the field by providing normative conclusions, an experimentally validated framework, and reproducible tools that can be immediately applied to the design of real-world photonic systems.

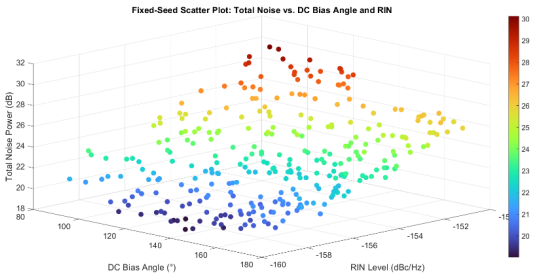

Fig. 11. Fixed-Seed scatter plot: total noise vs. DC bias angle and RIN

6 Conclusion

This paper deeply studies the linear modulation techniques and frequency conversion strategies in microwave photonic systems, focusing on the performance indicators of ROF links using MZMs. Through theory and simulation, this paper rigorously examines the effects of DC bias tuning, RIN, and PD optical power on key system parameters, namely noise figure, gain, and SFDR. Experiments show that strict control of modulation parameters, namely modulator bias angle and input optical power, can effectively suppress nonlinear effects and improve overall link performance.

Future research will more deeply integrate low-RIN laser sources, adaptive bias control strategies, and advanced digital signal processing techniques to further improve the performance and reliability of microwave photonic systems. In addition, the application of such optimized modulation and frequency conversion in 6G mobile backhaul and high-speed wireless access networks is another area worthy of further research and technology development.

References

[1] C.-T. Lin, J. Chen, S.-P. Dai, P.-C. Peng, S. Chi, Impact of Nonlinear Transfer Function and Imperfect Splitting Ratio of MZM on Optical Up-Conversion Employing Double Sideband with Carrier Suppression Modulation, Journal of Lightwave Technology 26(15)(2008) 2449-2459.

[2] H.-N. Parajuli, E. Udvary, A Vestigial sideband modulation scheme in radio over fiber system using electro-optic modulators, in: Proc. 2016 18th International Conference on Transparent Optical Networks, 2016.

[3] Y.-S. Gao, A.-J. Wen, Q.-W. Yu, N.-N. Li, G.-B. Lin, S.-Y. Xiang, L. Shang, Microwave Generation With Photonic Frequency Sextupling Based on Cascaded Modulators, IEEE Photonics Technology Letters 26(12)(2014) 1199-1202.

[4] S.-R. Moon, M. Sung, E.-S. Kim, J.-K. Lee, S.-H. Cho, J. Kim, RoF-based indoor distributed antenna system that can simultaneously support 5G mmWave and 6G terahertz services, Optics Express 30(2)(2022) 1521-1533.

[5] H.-M. El-Hageen, P.-G. Kuppusamy, A.-M. Alatwi, M. Sivaram, Z.-A. Yasar, A.-N.-Z. Rashed, Different modulation schemes for direct and external modulators based on various laser sources, Journal of Optical Communications 44(s1)(2023) s697-s706.

[6] A. Szasz, Therapeutic basis of electromagnetic resonances and signal-modulation, Open Journal of Biophysics 11(3)(2021) 314-350.

[7] S. Dev, K. Singh, R. Hosseini, A. Misra, M. Catuneanu, S. Preußler, T. Schneider, K. Jamshidi, Compact and Energy-Efficient Forward-Biased PN Silicon Mach–Zehnder Modulator, IEEE Photonics Journal 14(2)(2022) 6616507.1-6616507.7.

[8] W.-X. Ouyang, F. Teng, J.-H. He, X.-S. Fang, Enhancing the Photoelectric Performance of Photodetectors Based on Metal Oxide Semiconductors by Charge-Carrier Engineering, Advanced Functional Materials 29(9)(2019) 1807672.1-1807672.20.

[9] K. Xu, R.-X. Wang, Y.-T. Dai, F.-F. Yin, J.-Q. Li, Y.-F. Ji, J.-T. Lin, Microwave photonics: Radio-over-fiber links, systems, and applications, Photonics Research 2(4)(2014) B54-B63.

[10] B.-R. Song, L.-F. Zhang, X.-J. Qi, J.-R. Liu, C.-W. Zhang, Z.-P. Wang, Z.-M. Zhang, Measuring Boltzmann constant and electron charge based on circuit noise, Physics Experimentation 43(3)(2023) 43-49.

[11] H.-J. Zhou, W.-H. Yang, Z.-X. Li, X.-F. Li, Y.-H. Zheng, A bootstrapped, low-noise, and high-gain photodetector for shot noise measurement, Review of Scientific Instruments 85(1)(2014) 01311.1-01311.6.
[12] Q.-Y. Jin, Q.-Y. Feng, Z.-R. Wang, Analysis of passive intermodulation in cascaded connectors with transmit–receive systems, IET Microwaves, Antennas & Propagation 17(7)(2023) 518-525.
[13] R. Fattal, D. Lischinski, M. Werman, Gradient domain high dynamic range compression, Seminal Graphics Papers: Pushing the Boundaries 2(70)(2023) 671-678.
[14] S. Shin, U. Sharma, H. Tu, W. Jung, S.-A. Boppart, Characterization and Analysis of Relative Intensity Noise in Broadband Optical Sources for Optical Coherence Tomography, IEEE Photonics Technology Letters 22(14)(2010) 1057-1059.
[15] S.-M. Vaezi-Nejad, M. Cox, N. Cooper, Novel instrumentation for measurement of relative intensity noise, Transactions of the Institute of Measurement and Control 34(4)(2012) 437-486.
[16] L.-B. Kish, Thermal noise engines, Chaos, Solitons and Fractals: Applications in Science and Engineering: An Interdisciplinary Journal of Nonlinear Science 44(1/3)(2011) 114-121.
[17] P.-A. Morton, M.-J. Morton, High-Power, Ultra-Low Noise Hybrid Lasers for Microwave Photonics and Optical Sensing, Journal of Lightwave Technology 36(21)(2018) 5048-5057.
[18] C. Shen, T.-K. Ng, J.-T. Leonard, A. Pourhashemi, H.-M. Oubei, M.-S. Alias, S. Nakamura, S.P. DenBaars, J.S. Speck, A.Y. Alyamani, M.M. Eldesouki, B.S. Ooi, High-Modulation-Efficiency, Integrated Waveguide Modulator–laser Diode at 448 nm, ACS Photonics 3(2)(2016) 262-268.
[19] P. Ding, N. Chen, R.-X. Peng, Y.-C. Xiao, P.-F. Qu, Broadband Low-noise Microwave Optical Transmission Technology Based on Laser RIN Suppression, Semiconductor Optoelectronics 45(2)(2024) 269-273.